



Comparing of brain tumor diagnosis with developed local binary patterns methods

Mehmet Gül¹ · Yılmaz Kaya²

Received: 19 February 2023 / Accepted: 14 January 2024 / Published online: 22 February 2024
© The Author(s) 2024

Abstract

A brain tumor is one of the most lethal diseases that can affect human health and cause death. Invasive biopsy techniques are one of the most common methods of identifying brain tumor disease. As a result of this procedure, bleeding may occur during the procedure, which could harm some brain functions. Consequently, this invasive biopsy process may be extremely dangerous. To overcome such a dangerous process, medical imaging techniques, which can be used by experts in the field, can be used to conduct a thorough examination and obtain detailed information about the type and stage of the disease. Within the scope of the study, the dataset was examined, and this dataset consisted of brain images with tumors and brain images of normal patients. Numerous studies on medical images were conducted and obtained with high accuracy within the hybrid model algorithms. The dataset's images were enhanced using three distinct local binary patterns (LBP) algorithms in the developed model within the scope of the study: the LBP, step-LBP (nLBP), and angle-LBP (α LBP) algorithms. In the second stage, classification algorithms were used to evaluate the results from the LBP, nLBP and α LBP algorithms. Among the 11 classification algorithms used, four different classification algorithms were chosen as a consequence of the experimental process since they produced the best results. The classification algorithms with the best outcomes are random forest (RF), optimized forest (OF), rotation forest (RF), and instance-based learner (IBk) algorithms, respectively. With the developed model, an extremely high success rate of 99.12% was achieved within the IBk algorithm. Consequently, the clinical service can use the developed method to diagnose tumor-based medical images.

Keywords Brain Tumors · Deep Learning · Local Binary Patterns algorithms · Diagnosis · Classification

Abbreviations

LBP	Local binary patterns
nLBP	Step local binary patterns
α LBP	Angle local binary patterns
RF	Random forest
OF	Optimized forest
rf	Rotation forest
IBk	Instance-based learner
LGG	Low-grade gliomas
HGG	High-grade gliomas

GBM	Glioblastoma
CT	Computed tomography
PET	Positron emission tomography
MRI	Magnetic resonance imaging
CNS	Central nervous system
RF-EMF	Radiofrequency electromagnetic fields
ML-SVM	Multilayered support vector machine
GLRLM	Gray-level run length matrix
CS-LBP	Center-symmetric local binary pattern
DWT	Discrete wavelet transform
SP	Steerable pyramid
GLCM	Gray-level co-occurrence matrix
HLDP-GF	Hybrid local directional pattern with Gabor filter
FT-CNN	Fine-tuned convolutional neural networks
RGB	Red green blue
SMO	Sequential minimal optimization
RBF	Radial basis function
TP	True positive

✉ Mehmet Gül
mgul@sirnak.edu.tr

Yılmaz Kaya
yilmaz.kaya@batman.edu.tr

¹ Faculty of Engineering, Computer Engineering, Şırnak University, Şırnak, Turkey

² Faculty of Engineering, Computer Engineering, Batman University, Batman, Turkey

TN	True negative
FP	False positive
FN	False negative

1 Introduction

More than half of all cases of brain tumors are caused by gliomas [1]. Glioma primary brain tumors are divided into four groups according to symptoms: low-grade I and II gliomas (LGG) and high-grade III and IV gliomas (HGG) [2]. This extremely lethal tumor can occur at any age in various histological subregions. Additionally, a glioma tumor is an invasive tumor [3]. The glioblastoma (GBM) cells that cause the tumor can grow and spread very rapidly as they immerse in the healthy brain parenchyma and infiltrate into the surrounding tissues. In this circumstance, it increases the significance of the early diagnosis of brain tumor disease. A brain tumor can be detected with computed tomography (CT), positron emission tomography (PET), and magnetic resonance imaging (MRI) [4]. Among the brain's soft tissue imaging methods, MRI imaging produces better outcomes compared to other methods. The fact that there are billions of active cells in the brain tissue complicates the detection and treatment of the tumoral region in the event that a possible tumor forms. One of the leading causes of death in people recently is due to tumors in brain tissue. It has been determined that approximately 300,000 people worldwide apply to hospitals with complaints of brain tumors every year. More than 150 types of brain tumors have been identified in humans [5].

Approximately 700,000 people in the USA currently have a primary brain tumor, and another is expected to be diagnosed in 2022. Brain tumors can cause death, have a significant impact on quality of life, and alter everything for the patient and their relatives. Without distinction, brain tumors impact both sexes and all racial and ethnic groups of people [6]. A primary brain or spinal cord tumor originates from the brain or spinal cord. An estimated 25,050 adults (14,170 men and 10,880 women) in the USA were diagnosed with primary cancerous tumors in the brain and spinal cord in 2022. It is less than 1% of the probability of catching this type of tumor in a person's lifetime. Brain tumors account for 85 to 90% of all primary central nervous system (CNS) tumors. An estimated 308,102 people were diagnosed with a primary brain or spinal cord tumor in 2020. About 4170 children under the age of 15 were diagnosed with brain or CNS tumors in 2020 in the USA. This occurs when a tumor develops outside of the brain and

spreads to other parts of the body. Leukemia, lymphoma, melanoma, breast, kidney, and lung cancers are the most typical tumors that spread to the brain. Cancer in the brain and other nervous systems is the 10th leading cause of death for men and women. Globally, primary CNS and brain tumors were estimated to have been the leading cause of 251,329 fatalities in 2020.

The percentage of people who live for at least five years after the tumor is found is called the 5-year survival rate. It is almost 36% of the 5-year survival rate for people with a cancerous brain or CNS tumor in the USA. The 10-year survival rate is almost 31%. Age is a factor in overall survival rates after being diagnosed with a cancerous brain or CNS tumor. For those under the age of 15, the 5-year survival rate is almost 75%. For those between the ages of 15 and 39, the 5-year survival rate is close to 72%. The 5-year survival rate for people aged 40 and over is 21%. The type of brain or spinal cord tumor does, however, have a substantial effect on predicting survival rates. The consequences of your diagnosis should be discussed with your doctor. It is critical to remember that estimates of patients with brain tumors' chances of survival exist [7].

The fact that the brain tumor, which has a significant risk of death, is so dangerous makes it essential for early diagnosis and rapid initiation of treatment. Identification of the tumor area is extremely important. When the studies conducted in this case were analyzed, deep learning-based studies obtained very remarkable results. Among these studies conducted with deep learning, convolutional neural network methods such as AlexNet, VGG-Net, ResNet, and Google-Net draw attention [8]. The most prominent feature of the studies carried out with deep learning methods is that they have a strong feature extraction capacity [9–11]. Fuzzy edge detection and U-Net CNN classifications outperform traditional machine learning approaches, particularly when it comes to segmenting brain tumors [12]. Brain tumor components are primary and secondary metastases. Primary tumors occur in the CNS, while secondary tumors occur in the extracranial regions. The most common of the primary tumors is the GBM tumor. Secondary tumors occur when cancer cells, particularly those from the lung, breast, or kidney, metastasize to the brain [13].

The authors of the [14] study examined MRI images of brain tumor patients. The dataset used consisted of 86 images from the study. The obtained MRI images were applied separately to the LBP and Gabor wavelet transform methods, and impressive results were obtained. In the study, 0.93 foreground pixel precision and 0.98 background pixel precision results were obtained. In the study conducted by Sharif et al., the detection and segmentation of the tumor area in the brain soft tissue and the classification of the grades of the existing tumor areas were performed, respectively. A high success rate of 99% was

obtained from the complex datasets used in this study [14]. In another study, a dataset of brain tumor images was first processed with the LBP method and then re-evaluated with the multilayered support vector machine (ML-SVM). In the study, the accuracy rate was as high as 99.23% [15]. In 2016, another study was conducted to automate the detection of gliomas in 3D images. It obtained a high success accuracy rate and also performed the segmentation of the glioma tumor in 3D MRI images in the study in 2016 [16]. In another study carried out in 2020, a brain tumor detection study was carried out on MRI images. In this study, the gray-level run length matrix (GLRLM) method was initially applied to the images, and then, the center-symmetric local binary pattern (CS-LBP) method was applied. As a result of the study, a great example of success was revealed, with an accuracy rate of 94% [17].

The study, conducted by Gupta et al. in 2018, was on a classified glioma brain tumor. Within the scope of the study, the boundaries of the tumor were determined on 3D images by applying the discrete wavelet transform (DWT) and LBP methods together. In this study, a high success rate was obtained with an accuracy of 96% [18]. In another study conducted in 2019, feature extraction examined MRI images of brain tumor patients. Feature extraction was used together with the LBP method and the steerable pyramid (SP) method. In the conducted study, a high success rate was obtained with an accuracy rate of 97.67% [19]. Sharif et al. obtained quite remarkable results in 2019. Within the scope of the study, the tumor image dataset obtained from MRI imaging was subjected to a series of algorithms. Among the algorithms applied, there is also the LBP algorithm, and with the developed method, the researchers attained a high success rate of 98% [20]. In the study conducted in 2022, Başaran first evaluated the MRI dataset containing brain tumors with the gray-level co-occurrence matrix (GLCM) method. After the first evaluation, the images were enhanced with the LBP method. The results were re-evaluated with a fully connected layer of AlexNet, VGG16, EfficientNet, and ResNet50. A remarkable success rate of 98.22% was achieved in this study [21]. Researchers carried out another study in 2022 for extraction. Together, they used MRI tumor images to extract the texture, intensity, and shape features of brain tumors using the LBP and hybrid local directional pattern with Gabor filter (HLDP-GF) methods. In this study, a high success rate of 99.5% was achieved [22]. In another study conducted in 2022, a brain tumor dataset was obtained from two different hospitals in China: Nanfang Hospital in Guangzhou and Tianjin Medical University General Hospital in Tianjin. The dataset images were first enhanced with fine-tuned convolutional neural networks (FT-CNN) and LBP methods, which were applied separately. A high success rate of 98.7% was obtained in this study [23].

Within the scope of the conducted study, literature studies were carried out in the early diagnosis of brain tumors, and the diagnosis of brain tumors was successfully conducted with LBP algorithms. In this study, two new LBP algorithms were proposed based on the classical LBP method. The results obtained with the proposed LBP methods were re-evaluated with some classification algorithms, and all the results were compared. The study continues as Material and Methods, Results and Discussion, and Conclusion.

2 Material and methods

2.1 Dataset

The brain tumor dataset images were obtained from the public Kaggle website [24]. When the images of the dataset are examined, 45% of the images belong to healthy individuals, while the rest contain images of diseased individuals. Not all images in the dataset have certain resolution. Of the images with different image resolutions, 19% have a resolution of 512×512 pixels, 8% have a resolution of 225×225 pixels, and the remaining images have different pixel resolutions. Although the dataset containing brain tumors contains a large number of images, the images have different resolutions. In addition, 97% of the images in the dataset are in three color format (red green blue–RGB) while the rest are in gray format. The most important factor in achieving high success in deep learning-based applications is that the datasets included contain a large number of images. The dataset considered within the scope of the study includes 4600 brain MRI images of diseased and healthy individuals. The number of images in the dataset is considerable when some other studies in this field are examined. For example, the brain tumor segmentation (BraTS) challenge is the most common dataset used in studies on brain tumors. While the BraTS2021 challenge includes approximately 8000 MRI images, the BraTS2020 challenge includes approximately 2640 MRI images. This shows that there is a significant number of images in the dataset considered within the scope of the study. This situation is also important for our study (Fig. 1).

2.2 Block diagram of study

First, the dataset's brain tumor images were converted to 256×256 pixel sizes. The color presence of the images was checked, and if the images were in RGB format, they were converted to grayscale. After checking and conversion, the images were then converted to binary format. The binary format images in the dataset were then applied to

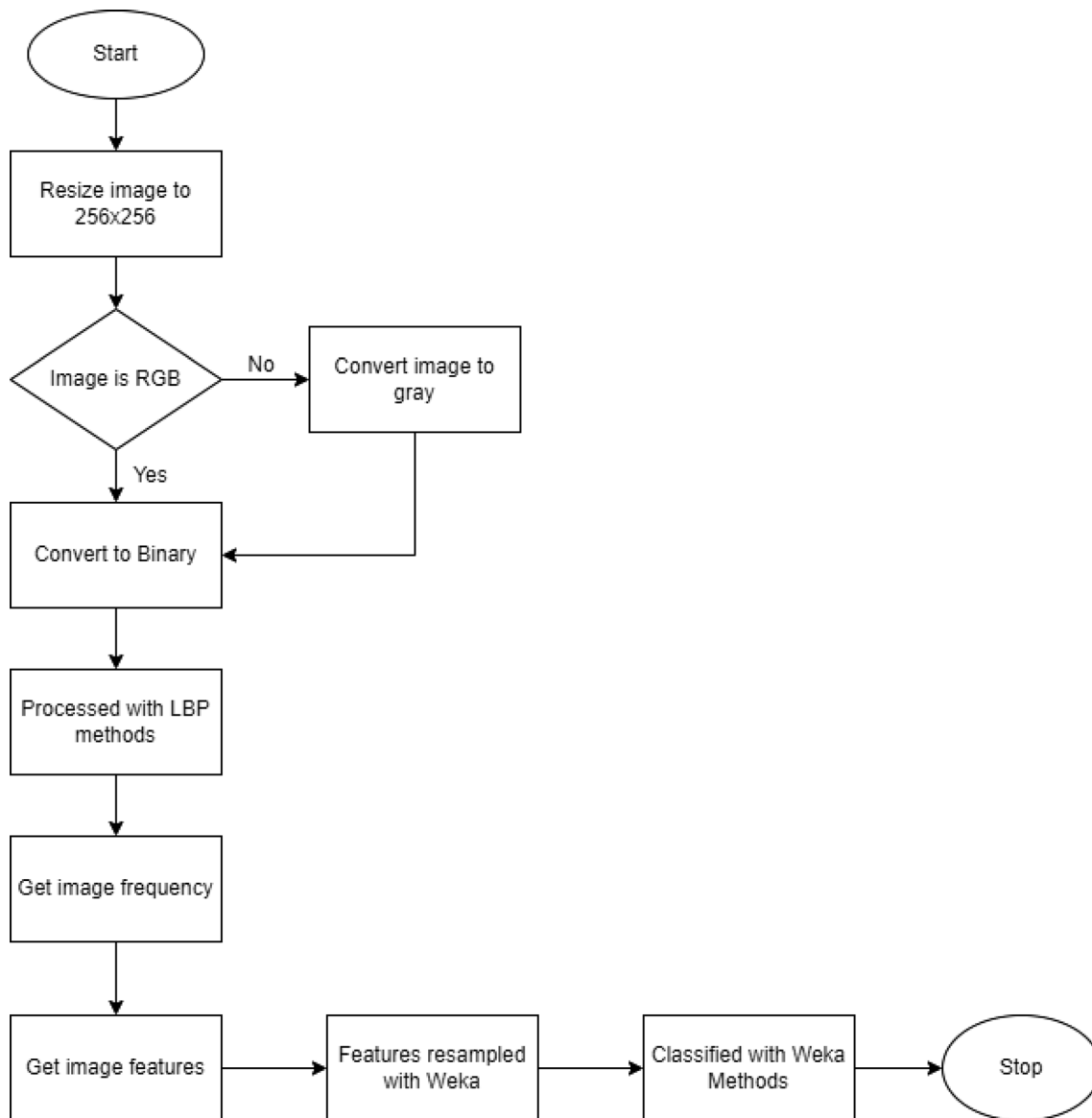


Fig. 1 Block Diagram

the LBP algorithms (LBP, nLBP and α LBP respectively). For that process, MATLAB software was used. The frequency values and features of the images enhanced with LBP methods were extracted. Following the frequency extraction process, the values of the retrieved images were applied to the resample function in the Weka software. Finally, some selected classification algorithms were applied for analysis in Weka software.

2.3 Feature extraction methods

Feature extraction is especially important for detecting and classifying the hidden details in the image. The feature extraction process helps maximize the similarity within the class and minimize the similarity between classes. At this

point, important information about the image is revealed. Vectors are obtained by subtracting the features. After this stage, vectors are used to train and test the data in the classification step [25].

2.3.1 Local binary pattern

To extract textural characteristics, one uses the local binary pattern (LBP) technique. There are numerous advantages obtained from the LBP method. At the beginning of these is a simple algorithm feature. It requires less computation compared to other algorithms. On the other hand, its insensitivity to different lighting intensities can be defined as another advantage [26]. The examination of texture has a critical place in the image processing process. In the

process of texture analysis, it is of particular importance to be able to adapt between different traditional statistical and structural models. This harmony can be provided by the LBP method. It is a fairly successful technique, especially when used to combat grayscale shifts brought on by things like variations in lighting in an image. Additionally, the LBP approach has a straightforward computational feature [27]. The LBP method’s formula (1) is as follows:

$$LBP_{P,R} = \sum_{i=0}^{P-1} s(g_i - g_c)2^i, s(x) = \begin{cases} 1 & x \geq 0 \\ 0 & x < 0 \end{cases} \quad (1)$$

P depicts as the neighbors of central pixel, R represents the radius of neighborhood, g_i is neighboring pixel intensity, and g_c is center pixel value.

The binary equivalent of the sub-image image calculated in Fig. 2 is $(10,111,001)_2$. When the binary equivalent is calculated as decimal, the equivalent of the Pc value in the sub-image is 185.

2.3.2 Local binary pattern with relationship of distance neighbors

Since the first use of the LBP method, numerous variations of LBP methods have been developed. The first of the two LBP algorithms that are proposed in this study operates on the fundamental principle of considering the eight adjacent pixels around the central pixel sequence. If $P_c = P_0, P_1, P_2, P_3, P_4, P_5, P_6,$ and P_7 pixels around the center pixel are bounced and processed instead of sequentially, a result different from the original LBP method will result.

In Fig. 3, it is shown according to the number of bounces. Instead of comparing according to the P_c center pixel in the sub-image, in the developed nLBP method, a relationship was established between eight pixels around the P_c .

According to Fig. 3, if the step parameter is one, then $P_c = S(P_0 > P_1), S(P_1 > P_2), S(P_2 > P_3), S(P_3 > P_4), S(P_4 > P_5), S(P_5 > P_6), S(P_6 > P_7), S(P_7 > P_0)$ relation is performed.

If the step parameter is two, then $P_c = S(P_0 > P_2), S(P_1 > P_3), S(P_2 > P_4), S(P_3 > P_5), S(P_4 > P_6), S(P_5 > P_7), S(P_6 > P_0), S(P_7 > P_1)$ relation is performed.

If the step parameter is three, then $P_c = S(P_0 > P_3), S(P_1 > P_4), S(P_2 > P_5), S(P_3 > P_6), S(P_4 > P_7), S(P_5 > P_0), S(P_6 > P_1), S(P_7 > P_2)$ relation is performed.

If the step parameter is four, then $P_c = S(P_0 > P_4), S(P_1 > P_5), S(P_2 > P_6), S(P_3 > P_7), S(P_4 > P_0), S(P_5 > P_1), S(P_6 > P_2), S(P_7 > P_3)$ relation is performed.

Thus, some changes were introduced in the classical LBP calculation;

$$S(P_i > P_j) = \begin{cases} 1 & \text{if } P_i > P_j \\ 0 & \text{if } P_i \leq P_j \end{cases} \quad (2)$$

was recalculated.

Considering the sub-image in Fig. 1 above as an example, the binary equivalent of step 1:

$P_c = S(36 > 221), S(221 > 129), S(129 > 80), S(80 > 145), S(145 > 190), S(190 > 219), S(219 > 168), S(168 > 36) = 01100011$; the decimal equivalent of the obtained value is 99.

Considering the sub-image in Fig. 1 above as an example, the binary equivalent of step 2:

$P_c = S(36 > 129), S(221 > 80), S(129 > 145), S(80 > 190), S(145 > 219), S(190 > 168), S(219 > 36), S(168 > 221) = 01000110$; the decimal equivalent of the obtained value is 70.

Considering the sub-image in Fig. 1 above as an example, the binary equivalent of step 3:

$P_c = S(36 > 80), S(221 > 145), S(129 > 190), S(80 > 219), S(145 > 168), S(190 > 36), S(219 > 221), S(168 > 129) = 01000101$; the decimal equivalent of the obtained value is 69.

Considering the sub-image in Fig. 1 above as an example, the binary equivalent of step 4:

$P_c = S(36 > 145), S(221 > 190), S(129 > 219), S(80 > 168), S(145 > 36), S(190 > 221), S(219 > 129), S(168 > 80) = 01001011$; the decimal equivalent of the obtained value is 75.

2.3.3 Local binary pattern with relationship of angle parameters

The main purpose of the LBP method is to perform texture analysis on the image. Different variants of the LBP

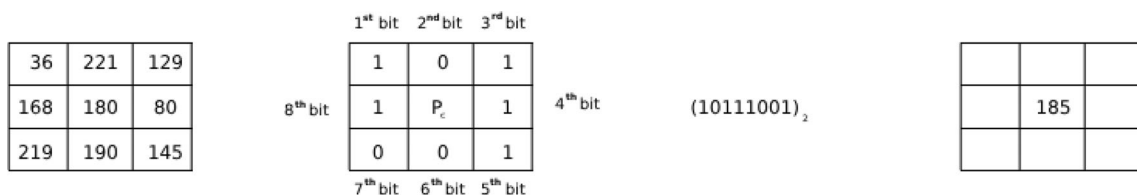


Fig. 2 Original LBP method calculation

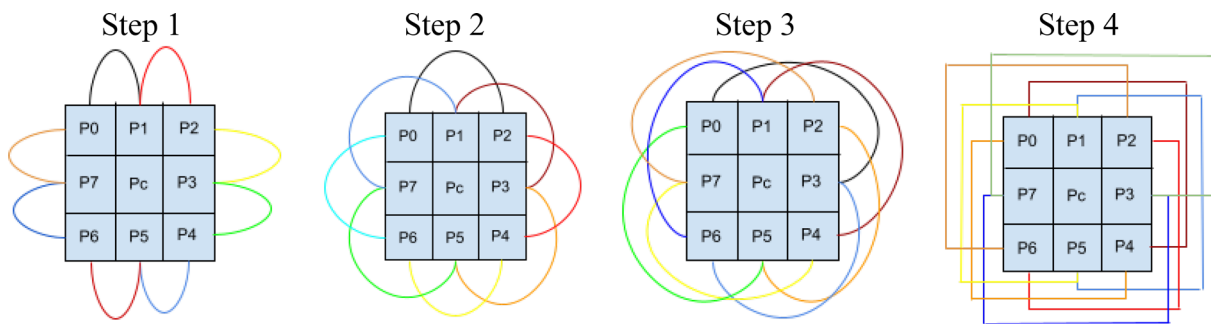


Fig. 3 Sub-image enhanced by step-LBP algorithm

method were developed during the tissue analysis process, and different results were obtained with the developed variants. In the scope of the study, the second method we will consider within the variant studies is the LBP method, which depends on the angle value. In Fig. 4, the angle-LBP (α LBP) approach is illustrated.

In the classical LBP method, the center pixel is compared with the eight neighboring pixels around it, while in the α LBP method, the calculation is performed on the two-way neighbor values above the determined angle value of the selected center pixel. The calculation formula of this developed approach is as follows:

$$\alpha\text{LBP} = \sum_{i=0}^P u(P_i - P_c)2^i \tag{3}$$

If it is performed an example calculation;

3 adjacent pixels considered for the value of $\alpha = 0$

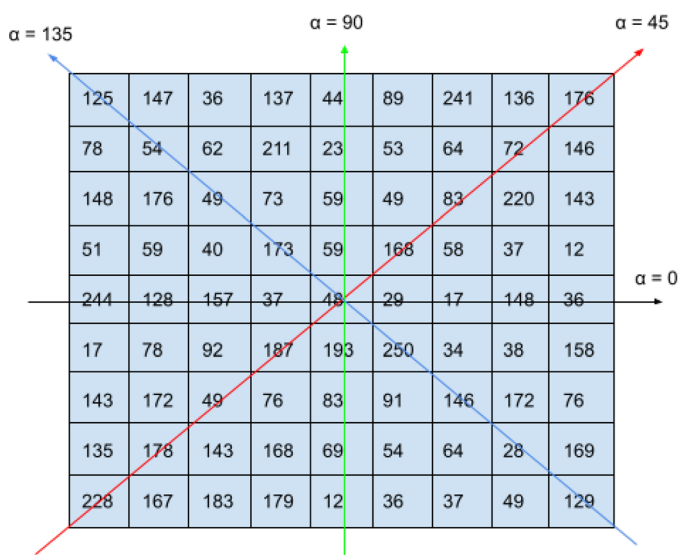
$P_c = S(48 > 244), S(48 > 128), S(48 > 157), S(48 > 37), S(48 > 29), S(48 > 17), S(48 > 148), S(48 > 36).$

is in the form. The binary equivalent of the obtained P_c value is 00011101 and the decimal equivalent corresponds to the $P_c = 29$ value.

4 adjacent pixels considered for the value of $\alpha = 45$

$P_c = S(48 > 228), S(48 > 178), S(48 > 49), S(48 > 187), S(48 > 166), S(48 > 83), S(48 > 72), S(48 > 176).$

is in the form. The binary equivalent of the obtained P_c value is 00000000 and the decimal equivalent corresponds to the $P_c = 0$ value.



$P_{7_{135}}$				$P_{7_{90}}$				$P_{7_{45}}$
	$P_{6_{135}}$			$P_{6_{90}}$			$P_{6_{45}}$	
		$P_{5_{135}}$		$P_{5_{90}}$		$P_{5_{45}}$		
			$P_{4_{135}}$	$P_{4_{90}}$	$P_{4_{45}}$			
P_{0_0}	$1P_{2_0}$	P_{2_0}	P_{3_0}	P_c	P_{4_0}	P_{5_0}	P_{6_0}	P_{7_0}
			$P_{3_{45}}$	$P_{3_{90}}$	$P_{3_{135}}$			
			$P_{2_{45}}$	$P_{2_{90}}$		$P_{2_{135}}$		
	$P_{1_{45}}$			$P_{1_{90}}$			$P_{1_{135}}$	
$P_{0_{45}}$				$P_{0_{90}}$				$P_{0_{135}}$

Fig. 4 The sub-image is enhanced by angle-LBP algorithm

5 adjacent pixels considered for the value of $\alpha = 90$

$P_c = S(48 > 12), S(48 > 69), S(48 > 83), S(48 > 193), S(48 > 59), S(48 > 59), S(48 > 23), S(48 > 44).$

is in the form. The binary equivalent of the obtained P_c value is 10,000,011 and the decimal equivalent corresponds to the $P_c = 131$ value.

6 adjacent pixels considered for the value of $\alpha = 135$

$P_c = S(48 > 129), S(48 > 28), S(48 > 146), S(48 > 250), S(48 > 173), S(48 > 49), S(48 > 54), S(48 > 125).$

is in the form. The binary equivalent of the obtained P_c value is 01000000 and the decimal equivalent corresponds to the $P_c = 64$ value. In this way, each time the angle changes, the α LBP method gives us a new pattern.

6.1 Classification methods

Weka software was another used software within the scope of this study. Weka software was developed by the University of Waikato and takes its name from the initials of the words “Waikato Environment for Knowledge Analysis.” Many of the most commonly used machine learning classification algorithms can be used on Weka software. Weka software was developed in Java language and also Java projects prepared can especially be easily uploaded. Weka software contains a series of comprehensive algorithms primarily for the purpose of data mining. These algorithms are especially used for feature selection, clustering, association rule learning, classification, and regression purposes [28]. In this section, a number of classification methods used on Weka software, especially within the scope of this study, are listed.

6.1.1 Instance-based learner

The instance-based learner (IBk) algorithm used in the Weka software corresponds to the K-nearest neighbor (KNN) algorithm used in other machine learning or deep learning software. The KNN algorithm identifies the training samples in the dataset with n-dimensional numerical features. Basically, when the KNN algorithm explores any sample in the dataset, it searches the pattern space for the k training samples closest to the sample being considered. In this way, the most common class assignment is performed among the k-nearest neighbors of the sample under consideration [29, 30]. Within the scope of this study, the K-nearest neighbor value was analyzed with the

IBk algorithm. Each sample that did not appear in the features extracted with the IBk algorithm used was compared with the existing ones using a distance criterion.

6.1.2 Random forest

The random forest algorithm is a substantial statistical training model. It performs well, particularly in small- and medium-sized datasets. It does not need large datasets like neural network algorithms. The bagging operation performs the averaging of the noisy but approximately unbiased models in the dataset, thus reducing its variance. Each tree in the random forest algorithm can capture any complex interaction structure in the data. Each tree benefits greatly from the average, as it has a noisy nature. On the other hand, when each tree produced by bagging is similarly distributed, the average expectation for all trees distributed is the same. Therefore, the goal of bagged and evenly dispersed trees is to have comparable distributions and aim to minimize variance. The only way to overcome this undesirable situation for the outcome is by reducing the variance [31].

6.1.3 Optimized forest

The optimized forest algorithm is based on the decision forest algorithm from the genetic algorithm family. In this manner, optimized forest selection with high accuracy and diversity is carried out to improve the optimized forest algorithm’s overall accuracy. Using the chromosome structure of the genetic algorithm, it is coded to form a population of 20 chromosomes. Furthermore, the generated chromosomes are also subjected to crossover and mutation processes using the roulette wheel technique. After the first stage, the elitist approach is used to successfully pick chromosomes. The top 20 chromosomes are chosen from a pool of 40 to avoid the algorithm’s chromosomes degrading. As a result of all these processes, a sequential search process is applied to obtain the best ensemble accuracy [32].

6.1.4 Rotation forest

The rotation forest algorithm is significantly different from the random forest algorithm, despite both being based on trees. The main difference is that a rotation forest transforms attributes into sets of principal components and uses a C4.5 decision tree. Unlike the rotation forest algorithm, where the features are sampled at the node for each tree, the rotation forest algorithm uses all the attributes for each tree. The features are randomly divided into a certain f dimension and the transformation is generated independently for each feature set. However, some of the samples

can be discarded and then sampled, modified to include a particular case forest. On a smaller dataset, a PCA model is created. The created model is then applied to all samples to create a new feature f , and the dataset is combined [33].

6.1.5 J48 decision tree

Classification is the process of constructing a class model from a set of records containing class labels. The decision tree algorithm, on the other hand, performs the process of finding out how the feature vector of a set of samples behaves. The class is created for each newly created example on the basis of training examples. This approach, which creates estimate criteria for the target variables, makes the critical distribution easy to understand. J48 is the development of ID3, an implementation of the C4.5 algorithm. In cases of possible overfitting, pruning is used as a firming tool. The purity of each leaf is prioritized in other classification algorithms, while in this method, rules are made to provide the precise identification of the data. The aim here is to gradually generalize a decision tree until the algorithm achieves a balance between adaptability and precision [34].

6.1.6 Multilayer perceptron

It is the best-known and most commonly used neural network algorithm. There is no loop in this example. Usually, signals are only transferred in one direction inside the network, from input to output. The output of each neuron does not affect the neuron itself; however, forward data flows. This type of architecture is called feedforward, and there are hidden layers that are not directly connected to the environment. It can be in a feedback structure that incorporates reaction connections and provides data transmission in both directions due to its network structure. Such networks have the potential to be incredibly powerful and complicated. The network is dynamic until it reaches equilibrium. Multiple layers may indicate that decision areas need to be more sophisticated. A single-layer, single-input sensor creates decision regions in the form of half-planes. Each neuron in another layer added to the network serves as a standard sensor for the outputs of the front-layer neurons. In this case, the output of the network can predict the convex decision regions formed by the intersection of the half-planes formed by the neurons [35].

6.1.7 Simple logistic

This algorithm, sometimes referred to as “logit regression” or “logit model,” is a mathematical method that uses algebra to determine the likelihood of an occurrence based on statistical data. Logistic regression assigns 1 to event

occurrence and 0 to non-occurrence. A value of 1 is indicated for an event’s occurrence and 0 for its non-occurrence. For instance, a student receives a score of 1 for passing the exam and a score of 0 for failing it. This situation is also known as binomial logistic regression [36].

6.1.8 Multilayer perceptron

It is a feedforward neural network algorithm that is used to distinguish data that cannot be separated linearly. Moreover, complicated functions can be modeled with this algorithm, and it is a widely used supervised learning method that does not ignore irrelevant inputs or noise. Its structure allows for the possibility of several layers. Each node represents a neuron with a nonlinear activation function. As it is most commonly known, it consists of an input layer, a hidden layer, and an output layer. The movement is only in a forward direction, from input nodes to hidden nodes and then to output nodes [37].

6.1.9 Sequential minimal optimization

Sequential minimal optimization (SMO) is a simple algorithm that solves any SVM quadratic programming (QP) problem without the need for extra matrix storage. Its sensitivity is thus lower than that of digital cutoff probes. It also has the ability to quickly solve problems without using any numerical QP optimization steps. The SMO algorithm uses Osuna’s theorem to perform the convergence operation. In this method, a general QP problem is decomposed into smaller QP problems. Unlike the more commonly used methods, SMO chooses to solve even the smallest possible optimization problem at every step. Rather than calling an entire QP library routine, the inner loop of the algorithm helps to accomplish this in a relatively short amount of C code. Even though the algorithm method solves more optimization sub-problems, the QP problem is solved quickly because each sub-problem is solved so quickly. Aside from this, SMO does not require additional matrix storage. As a result, large-scale issues like very large SVM training difficulties may be accommodated on any normal workstations or PC RAM [38].

6.1.10 Radial basis function

The radial basis function (RBF) classifier is an algorithm with a feedforward network structure used as a supervised training algorithm. The activation function is typically configured with a single layer of hidden units selected from a class of functions called core functions. Although the RBF algorithm has many characteristics with regard to back propagation, it also has several advantages. Although it trains more quickly than backpropagation networks, the

behavior of the single hidden layer is the key differentiator between the two. Instead of using the RBF algorithm's sigmoidal or S-shaped activation function, the hidden units in the RBF network use a Gaussian or other fundamental kernel function. Each created hidden unit generates a rating score to be able to match between its weights or centers associated with the input vector [39].

6.1.11 Decision table

This method enables the information in the tables to be used in an algorithmic way. The table may contain more than one land state. This situation changes according to the needs and expectations of the users. Even though decision tables are a traditional approach, they may be transformed into a unique, practical, and efficient tool that aids in decision making when coupled with contemporary design and management techniques. It is easy and understandable to define the actions to be taken after the conditions in the tables are met. The most fundamental function of the tables is to provide a solution to a problem. Tables demonstrate how cause (conditions) and effect (actions) are related. The biggest advantage of decision tables is the possibility of presenting complex relationships in a clear and transparent way. The most basic condition for the creation of decision tables is "If..., then..." [40].

6.2 Experimental test

The confusion matrix was used in the performance evaluation of the results of the experimental study. In the confusion matrix, the target attribute estimations and actual values are compared. The matrix used is summarized with the numerical values of the correct and incorrect prediction numbers. The actual values are represented by the columns in the generated matrix, while the rows represent a predicted class. In the resultant matrix, true positive (TP) and true negative (TN) are correctly predicted values in the model, while false positive (FP) and false negative (FN) are incorrectly predicted values in the model. Accuracy, sensitivity, specificity, precision, and F-Score values are calculated from this matrix. The following equations show the calculations of TP, TN, FP, and FN, respectively. The harmonic average of the F-Score precision and recall values is produced once all these values have been received.

$$\text{Accuracy(Acc)} = \frac{TP + TN}{TP + TN + FP + FN} \quad (4)$$

$$\text{Sensitivity(Se)} = \frac{TP}{TP + FN} \quad (5)$$

$$\text{Specificity(Sp)} = \frac{TN}{TN + FP} \quad (6)$$

$$\text{Precision(Prec)} = \frac{TP}{TP + FP} \quad (7)$$

$$\text{Fscore(F - Sc)} = \frac{2TP}{2TP + FP + FN} \quad (8)$$

7 Results and discussion

7.1 Results

The images in the dataset are required to preprocess because the images in the dataset are not all the same size or in the same color format. After the preprocessing step, the images in the dataset had a dimension of 256×256 pixels. The images' color formats were converted to grayscale formats. After all the preprocessing steps, the images were altered to the proper size and format. The images were converted into a single-color format and uniform size. After that, these were processed by the LBP methods. All images obtained from the dataset were first preprocessed and then subjected to two LBP algorithms developed alongside the classic LBP algorithm.

Sample images of patients with brain tumor disease and healthy individuals from the raw images in the dataset are given below. The images of the sample images handled in the dataset, which are formed as a result of image processing, are also shown in Fig. 5.

Within the scope of the study, the images of the brain tumor dataset obtained from the Kaggle website were enhanced with three different LBP methods. First, the results were obtained from the images processed with the classical LBP method, and then, the images were improved again with the newly developed nLBP and α LBP methods.

When the results in Table 1 are examined in detail, there are two different LBP algorithms developed by taking the classical LBP algorithm as a reference. Separately, quite

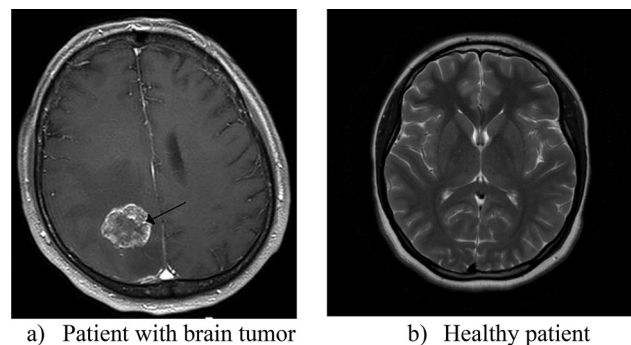


Fig. 5 The sample image in the dataset

Table 1 The results of correctly classified instance obtained of LBP, α -LBP, and nLBP algorithms

Preprocessing	Algorithms	α -LBP				LBP	nLBP			
		0	45	90	135		1	2	3	4
Resample + Smote	RF	97.6223	96.9044	96.9643	97.1587	96.9942	97.4278	97.1288	96.6951	96.1268
	OF	97.5624	96.9643	96.9344	97.0241	97.0689	97.3979	97.0689	96.5605	96.052
	IBk	98.8336	98.8485	98.5195	98.9532	99.0878	99.1177	98.0435	98.8485	98.5046
	RF	96.6801	96.0072	96.6054	95.9474	96.2764	96.6801	95.3913	95.9773	95.7679
	J48	92.792	91.7302	92.9864	91.8349	92.5079	93.3752	92.8219	91.9545	92.1938
	MLP Classifier	89.5319	87.9468	90.6535	87.528	91.2218	92.3284	89.0683	91.2367	86.7205
	Multilayer perceptron	90.6535	79.4377	79.3779	82.309	88.6048	90.2198	85.6886	83.6549	84.3278
	SMO	84.5521	83.8642	86.3915	83.4904	84.8662	87.0645	83.266	85.7186	77.0001
	Simple Logistic	83.8642	81.8902	84.2979	81.8753	81.9949	85.0307	81.2023	82.9071	77.5236
	RBF Classifier	84.1483	82.8174	85.6737	81.8753	83.9988	86.227	81.0079	84.7615	81.1575
	DT	82.5781	81.636	81.5164	81.0079	80.7088	82.4735	81.5014	78.8694	82.967

impressive outcomes were produced in the current algorithms built. Within the scope of the study, the highest success rate was obtained by re-evaluating the results obtained from the nLBP algorithm with the IBk classification algorithm used in Weka software. In general, it can be seen that the IBk algorithm performs successful classification in re-evaluating the results obtained from all three algorithms. When examined in general terms, it was determined that the results obtained with random forest and optimized forest classification algorithms were the second most successful classification algorithm. The rotation forest and J48 classification algorithms produced results with a success rate of more than 90%. The DT classification method produced the worst successful classification result in the investigation. Among the other categorization algorithms tested in the experimental investigation, success rates ranged between 80 and 90 percent.

Image classification was applied to all the results obtained as a result of all three studies. After the preprocessing stage, different results were obtained by changing the four angle values in the α LBP algorithm. The fifth result was obtained from the dataset subjected to the classical LBP algorithm. In the last stage, four different result values were obtained from four different values in the nLBP algorithm. The sample results are shown in Fig. 6. On the other hand, it is shown that there are nine different results for the healthy individual MRI image in the dataset in Fig. 7. All nine LBP and developed LBP results obtained were subjected to 11 different classification algorithms separately.

The four classification algorithms that give the best results are the random forest, optimized forest, IBk and rotation forest algorithms, respectively. All nine results

obtained were subjected to 11 different algorithms, and a total of 99 different results are given in Table 1.

When all the results obtained within the scope of the study were examined, the most successful results were obtained from the nLBP algorithm derived from the LBP algorithm. Among the 11 algorithms used for classification, the highest evaluation result was obtained with the IBk classification algorithm. Other successful results obtained by evaluating the nLBP algorithm values, such as ROC, recall and f-measure, are given in Table 2.

The results of this study are shown in Fig. 8. In the confusion matrix, the actual and predicted values are displayed. The power of the proposed method in confusion matrix is shown from another perspective.

7.2 Discussion

The results obtained from other studies using the same dataset are shown in Table 3. Table 3 shows the obtained results with the same dataset. The CNN algorithm was used in two different studies, and the results were close. High success results were obtained in these studies, especially those developed using the CNN algorithm and deep convolutional networks. Within the scope of the study, the images in the dataset containing brain tumors obtained from the Kaggle webpage were enhanced with the LBP, nLBP and α LBP algorithms. The highest accuracy rate was obtained with the nLBP algorithm in step 1. The highest accuracy rate obtained in the study was 99.12%. The study was written in MATLAB software, and the results were re-evaluated via Weka software.

Four different results were obtained by each nLBP and α LBP according to variables. The last result was obtained by the LBP algorithm. The variables of α LBP are 0, 45, 90

Fig. 6 Images created by the α LBP method according to different α value

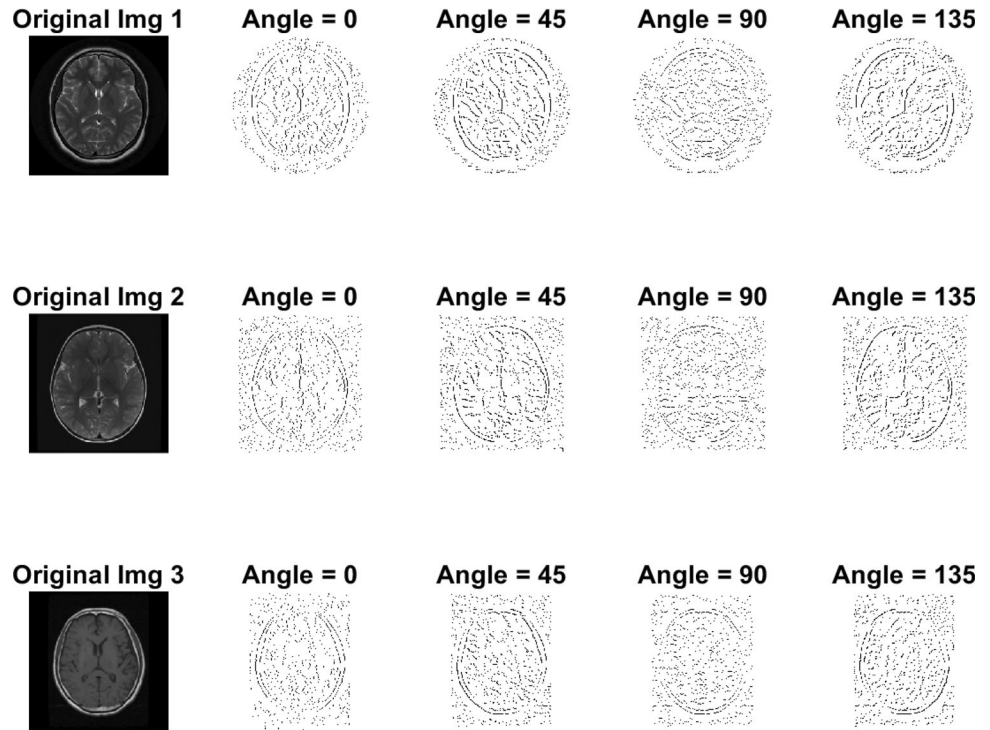
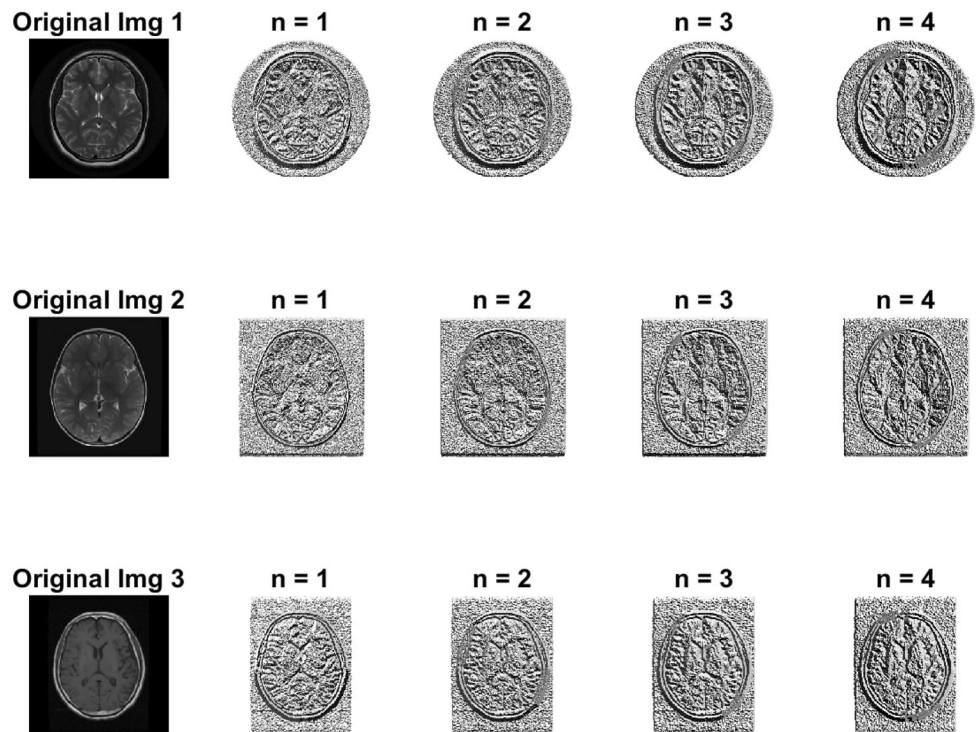


Fig. 7 Images created by the nLBP method according to different d values. **a** meningioma, **b** glioma, **c** pituitary

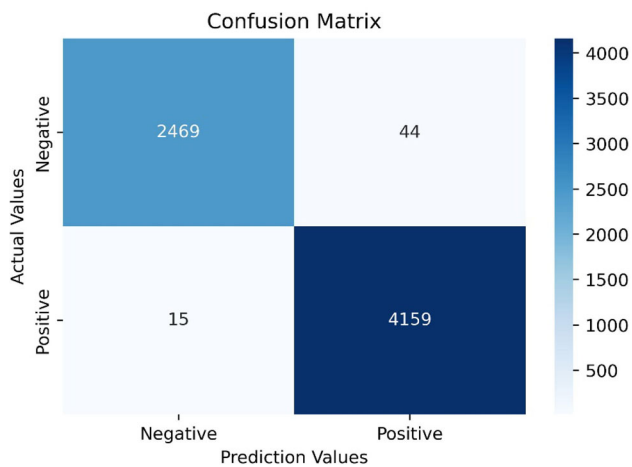


and 135 degrees, and the variables of nLBP are 1 to 4. Within the scope of the study, nine different evaluation results were obtained. The experimental results obtained with MATLAB software were preprocessed via Weka software by resample algorithm. After preprocessing, it was subjected to 11 different algorithms. Out of 11

different classification algorithms, it was chosen four that gave the most successful results that were determined. All the results obtained are shown in Table 1. The purpose of doing this is to perform the experimental work that will achieve the highest accuracy.

Table 2 Detailed accuracy by class

Used algorithm	Number of images	TP	FP	Pre	Recall	F-Measure	MCC	ROC	PRC	Class
nLBP (step 1)	4600	0.982	0.004	0.994	0.982	0.988	0.981	0.992	0.987	0
		0.996	0.018	0.990	0.996	0.993	0.981	0.992	0.992	1
		0.991	0.012	0.991	0.991	0.981	0.981	0.992	0.990	

**Fig. 8** Confusion matrix**Table 3** The other results obtained with the same dataset [41]

Used algorithms	Accuracy
CNN + VGG16—VGG19	%99
CNN + DenseNet121	%99
CNN	%99
CNN	%98.97

The results were obtained from the four successful classification algorithms that gave the highest results after the preprocess was evaluated. When the results were examined, the best results were obtained from the IBk classification algorithm; these ones are close to each other between the step 1 parameter in the nLBP and the classical LBP algorithm. While the result obtained from the classical LBP algorithm was subjected to the IBk classification, the success rate was 99.09%, while the success rate obtained by subjecting the results obtained from the nLBP algorithm to the IBk classification was 99.12%. The results obtained as a result of the study were preprocessed in Weka software and subjected to classification algorithms. The most successful classification result in the study was obtained with the IBk algorithm (Table 4).

Table 4 The results of related works of LBP algorithms studies

Studies	Methods	Acc	Year
[14]	LBP + Gabor Wavelet Transform	%98	2019
[15]	LBP + ML-SVM Classifier	%99.23	2022
[16]	LBP + Histogram Orientation Gradient	%93	2016
[17]	GLRLM & CS-LBP + classification Adopting Neural Network (ANN)	%94	2022
[18]	DWT + LBP	%96	2018
[19]	LBP + steerable pyramid	%97.67	2019
[20]	LBP + histogram of oriented gradients geometrical	%95	2019
[21]	Gray-level co-occurrence matrix + LBP traditional + AlexNet, VGG16, EfficientNet, ResNet50 CNN models	%98.22	2022
[22]	LBP + HLDP-GF techniques	%99.6	2022
[23]	Histogram of oriented gradients + LBP	%98.7	2022
This study	nLBP + IBk	%99.12	

8 Conclusion

Within the scope of the study, analysis was carried out on a comprehensive dataset containing images of brain tumor patients and images of healthy individuals. The main purpose of the analysis is to accurately identify images of brain tumor patients at an early stage with deep learning and machine learning-based algorithms. In this study, MRI images obtained on the dataset were enhanced with nLBP and α LBP algorithms based on the classical LBP algorithm. Since its development, the local binary pattern algorithm has developed numerous variants that have gained ground in image enhancement studies. Although there are many different algorithms developed based on the local binary patterns algorithm, it is reported that impressive results are obtained in many of these algorithms. The results obtained with the nLBP and α LBP algorithms developed within the scope of the study were re-evaluated using Weka software, which uses machine learning algorithms especially for data mining tasks. The images were first preprocessed and then re-evaluated with other classification algorithms. An extremely high success rate was achieved in the reclassification process. It was determined that IBk, random forest, optimized forest and rotation forest algorithms contributed

positively to the feature results obtained with LBP, nLBP and α LBP algorithms. When the results obtained were examined, the most successful result was obtained by determining the first step of the nLBP algorithm and using the IBk classification algorithm. One of the most important outcomes of the study is the further development of the successful results obtained within its scope. As part of future research, model training will be carried out with various datasets of MR images of brain tumors and efforts will be made to develop it further.

Funding Open access funding provided by the Scientific and Technological Research Council of Türkiye (TÜBİTAK).

Data availability The datasets generated during and/or analyzed during the current study are available in the Kaggle repository [24].

Declarations

Conflict of interest The authors declare no conflict of interest, financial or otherwise.

Open Access This article is licensed under a Creative Commons Attribution 4.0 International License, which permits use, sharing, adaptation, distribution and reproduction in any medium or format, as long as you give appropriate credit to the original author(s) and the source, provide a link to the Creative Commons licence, and indicate if changes were made. The images or other third party material in this article are included in the article's Creative Commons licence, unless indicated otherwise in a credit line to the material. If material is not included in the article's Creative Commons licence and your intended use is not permitted by statutory regulation or exceeds the permitted use, you will need to obtain permission directly from the copyright holder. To view a copy of this licence, visit <http://creativecommons.org/licenses/by/4.0/>.

References

- Nie J et al (2009) Automated brain tumor segmentation using spatial accuracy-weighted hidden Markov Random Field. *Comput Med Imaging Graph* 33(6):431–441. <https://doi.org/10.1016/j.compmedimag.2009.04.006>
- Bakas S, et al. (2018). Identifying the best machine learning algorithms for brain tumor segmentation, progression assessment, and overall survival prediction in the BRATS challenge. arXiv preprint arXiv:1811.02629..
- Essadike A, Ouabida E, Bouzid A (2018) Brain tumor segmentation with Vander Lugt correlator based active contour. *Comput Methods Programs Biomed* 160:103–117. <https://doi.org/10.1016/j.cmpb.2018.04.004>
- Havaei M et al (2017) Brain tumor segmentation with deep neural networks. *Med Image Anal* 35:18–31. <https://doi.org/10.1016/j.media.2016.05.004>
- Nayak DR, Padhy N, Mallick PK, Zymbler M, Kumar S (2022) Brain tumor classification using dense efficient-net. *Axioms* 11(1):34. <https://doi.org/10.3390/axioms11010034>
- Pichaiavel M, Anbumani G, Theivendren P, Gopal M (2022) An overview of brain tumor, in *brain tumors*. IntechOpen. <https://doi.org/10.5772/intechopen.100806>
- Siegel RL, Miller KD, Fuchs HE, Jemal A (2022) Cancer statistics, 2022. *CA Cancer J Clin* 72(1):7–33. <https://doi.org/10.3322/caac.21708>
- Jiang Y, Zhang Y, Lin X, Dong J, Cheng T, Liang J (2022) SwinBTS: a method for 3D multimodal brain tumor segmentation using swin transformer. *Brain Sci* 12(6):797. <https://doi.org/10.3390/brainsci12060797>
- Esteva A et al (2017) Dermatologist-level classification of skin cancer with deep neural networks. *Nature* 542(7639):115–118. <https://doi.org/10.1038/nature21056>
- Gulshan V et al (2016) Development and validation of a deep learning algorithm for detection of diabetic retinopathy in retinal fundus photographs. *JAMA* 316(22):2402. <https://doi.org/10.1001/jama.2016.17216>
- Hu J, Shen L, Sun G (2018). Squeeze-and-excitation networks. In: Proceedings of the IEEE conference on computer vision and pattern recognition (pp. 7132-7141).
- Maqsood S, Damasevicius R, Shah FM (2021). An efficient approach for the detection of brain tumor using fuzzy logic and U-NET CNN classification. In: Computational Science and Its Applications–ICCSA 2021: 21st International Conference, Cagliari, Italy, September 13–16, 2021, Proceedings, Part V 21 (pp. 105-118). Springer International Publishing. https://doi.org/10.1007/978-3-030-86976-2_8.
- Schaettler MO et al (2022) Characterization of the genomic and immunologic diversity of malignant brain tumors through multi-sector analysis. *Cancer Discov* 12(1):154–171. <https://doi.org/10.1158/2159-8290.CD-21-0291>
- Amin J, Sharif M, Raza M, Saba T, Anjum MA (2019) Brain tumor detection using statistical and machine learning method. *Comput Methods Programs Biomed* 177:69–79. <https://doi.org/10.1016/j.cmpb.2019.05.015>
- Kolla M, Mishra RK, Zahoor UI, Huq S, Vijayalata Y, Gopalachari MV, Siddiquee KA (2022) CNN-based brain tumor detection model using local binary pattern and multilayered SVM classifier. *Comput Int Neurosci* 2022:9015778–9015778. <https://doi.org/10.1155/2022/9015778>
- Abbasi S, Tajeripour F (2017) Detection of brain tumor in 3D MRI images using local binary patterns and histogram orientation gradient. *Neurocomputing* 219:526–535. <https://doi.org/10.1016/j.neucom.2016.09.051>
- Mudda M, Manjunath R, Krishnamurthy N (2022) Brain tumor classification using enhanced statistical texture features. *IETE J Res* 68(5):3695–3706. <https://doi.org/10.1080/03772063.2020.1775501>
- Gupta M, Rajagopalan V, Rao BVVSNP (2019) Glioma grade classification using wavelet transform-local binary pattern based statistical texture features and geometric measures extracted from MRI. *J Exp Theor Artif Intell* 31(1):57–76. <https://doi.org/10.1080/0952813X.2018.1518997>
- Kale VV, Hamde ST, Holambe RS (2019) Brain disease diagnosis using local binary pattern and steerable pyramid. *Int J Multimed Inf Retr* 8(3):155–165. <https://doi.org/10.1007/s13735-019-00174-x>
- Sharif M, Amin J, Nisar MW, Anjum MA, Muhammad N, Ali Shad S (2020) A unified patch based method for brain tumor detection using features fusion. *Cogn Syst Res* 59:273–286. <https://doi.org/10.1016/j.cogsys.2019.10.001>
- Başaran E (2022) A new brain tumor diagnostic model: Selection of textural feature extraction algorithms and convolution neural network features with optimization algorithms. *Comput Biol Med* 148:105857. <https://doi.org/10.1016/j.compbiomed.2022.105857>
- Sasank VVS, Venkateswarlu S (2022) Hybrid deep neural network with adaptive rain optimizer algorithm for multi-grade brain tumor classification of MRI images. *Multimed Tools Appl* 81(6):8021–8057. <https://doi.org/10.1007/s11042-022-12106-9>

23. Zahoor MM, Qureshi SA, Khan A, Rehman AU, Rafique M (2022). A novel dual-channel brain tumor detection system for MR images using dynamic and static features with conventional machine learning techniques. *Waves in Random and Complex Media*, <https://doi.org/10.1080/17455030.2022.2070683>.
24. “Brian Tumor Dataset,” <https://www.kaggle.com/datasets/preetviradiya/brian-tumor-dataset>.
25. Ningtyas AD, Nababan EB, Efendi S (2022) Performance analysis of local binary pattern and k-nearest neighbor on image classification of fingers leaves. *Int J Nonlinear Anal Appl* 13(1):1701–1708
26. Haghnegahdar AA, Kolahi S, Khojastepour L, Tajeripour F (2018) Diagnosis of tempromandibular disorders using local binary patterns. *J Biomed Phys Eng* 8(1):87–96
27. Ojala T, Pietikäinen M, Harwood D (1996) A comparative study of texture measures with classification based on featured distributions. *Pattern Recognit* 29(1):51–59. [https://doi.org/10.1016/0031-3203\(95\)00067-4](https://doi.org/10.1016/0031-3203(95)00067-4)
28. E Frank *et al.*, (2009) Weka-A Machine Learning Workbench for Data Mining, In: *Data Mining and Knowledge Discovery Handbook*, Boston, MA: Springer US, https://doi.org/10.1007/978-0-387-09823-4_66.
29. Rahman Ahad MdA, Islam MdN, Jahan I (2016) Action recognition based on binary patterns of action-history and histogram of oriented gradient. *J Multimodal User Interfaces* 10(4):335–344. <https://doi.org/10.1007/s12193-016-0229-4>
30. Han J, Kamber M, and Pei J, *Data Mining Concepts and Techniques*, 3rd ed. 2012.
31. Ionita I (2016) Data mining technique for e-learning. *J Appl Comput Sci Math* 10(2):26–31. <https://doi.org/10.4316/JACSM.201602004>
32. R Caruana A Niculescu-Mizil, (2006) An empirical comparison of supervised learning algorithms. In: *Proceedings of the 23rd international conference on Machine learning - ICML '06*, New York, New York, USA: ACM Press, 161–168, <https://doi.org/10.1145/1143844.1143865>.
33. Adnan MN, Islam MZ (2016) Optimizing the number of trees in a decision forest to discover a subforest with high ensemble accuracy using a genetic algorithm. *Knowl Based Syst* 110:86–97. <https://doi.org/10.1016/j.knosys.2016.07.016>
34. IA Jimoh, I Ismaila, M Olalere, (2019) Enhanced decision Tree-J48 With SMOTE machine learning algorithm for effective bot-net detection in imbalance dataset. In: *2019 15th International Conference on Electronics, Computer and Computation (ICECCO)*, IEEE, 1–8. <https://doi.org/10.1109/ICECCO48375.2019.9043233>.
35. Gardner MW, Dorling SR (1998) Artificial neural networks (the multilayer perceptron)—a review of applications in the atmospheric sciences. *Atmos Environ* 32(14–15):2627–2636. [https://doi.org/10.1016/S1352-2310\(97\)00447-0](https://doi.org/10.1016/S1352-2310(97)00447-0)
36. Hsieh FY, Bloch DA, Larsen MD (1998) A simple method of sample size calculation for linear and logistic regression. *Stat Med* 17(14):1623–1634. [https://doi.org/10.1002/\(SICI\)1097-0258\(19980730\)17:14%3c1623::AID-SIM871%3e3.0.CO;2-S](https://doi.org/10.1002/(SICI)1097-0258(19980730)17:14%3c1623::AID-SIM871%3e3.0.CO;2-S)
37. Tang J, Deng C, Huang G-B (2016) Extreme learning machine for multilayer perceptron. *IEEE Trans Neural Netw Learn Syst* 27(4):809–821. <https://doi.org/10.1109/TNNLS.2015.2424995>
38. Nakanishi KM, Fujii K, Todo S (2020) Sequential minimal optimization for quantum-classical hybrid algorithms. *Phys Rev Res* 2(4):043158. <https://doi.org/10.1103/PhysRevResearch.2.043158>
39. Buhmann MD (2000) Radial basis functions. *Acta Numer* 9:1–38. <https://doi.org/10.1017/S0962492900000015>
40. Baesens B, Setiono R, Mues C, Vanthienen J (2003) Using neural network rule extraction and decision tables for credit-risk evaluation. *Manage Sci* 49(3):312–329. <https://doi.org/10.1287/mnsc.49.3.312.12739>
41. Kaggle, “novel dual-channel brain tumor detection system for MR images .”

Publisher's Note Springer Nature remains neutral with regard to jurisdictional claims in published maps and institutional affiliations.